Stable cerium isotopes as a tracer of oxidation reactions

Pierre Bonnand, Maud Boyet, Chantal Bosq

Geochemical Perspectives Letters

Stable cerium isotopes as a tracer of oxidation reactions

P. Bonnand[1,2*], M. Boyet[1], C. Bosq[1]

OPEN ACCESS

https://doi.org/10.7185/geochemlet.2340

Abstract

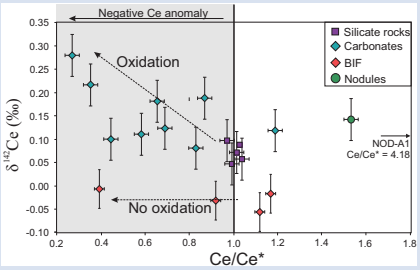

Redox conditions in past oceans have attracted significant interest and many proxies have been used to probe redox changes through time. For example, the redox dependent behaviour of Ce, resulting in negative or positive elemental Ce anomalies, has been widely used. More recently, mass dependent Ce isotopic variations have been proposed as a powerful tool to study Ce oxidation in natural environments. In this study, we demonstrate, for the first time, that Ce isotopes are fractionated during oxidation reaction, confirming the utility of Ce isotopes to study redox reactions. This result suggests that seawater Ce isotopic composition should be fractionated toward heavy values relative to the continental crust. Measured natural rock samples (carbonates, banded iron formations and Mn nodules) have variable Ce isotopic compositions, ranging from −0.055 ± 0.045 ‰ to +0.280 ± 0.045 ‰. The relation between Ce elemental anomalies and Ce isotopic composition in carbonate rocks suggest that mass dependent Ce isotopes can be used to distinguish elemental anomalies produced by oxidation reactions from those produced by other processes. Coupled with La-Ce chronology, mass dependent Ce isotope analysis is a very powerful tool to study redox reactions in past oceans.

Received 7 July 2023 | Accepted 22 November 2023 | Published 18 December 2023

Introduction

The oxygenation of the atmosphere and oceans during Earth history has attracted significant interest in the scientific community. Over geological time, Earth's surface environments experienced dramatic evolution in prevailing redox conditions, as the concentration of atmospheric molecular oxygen (O_2) increased from levels of less than 1 part per million by volume before 2.45 Ga to 21 % by volume today. While the exact drivers continue to be debated, the accumulation of atmospheric oxygen ultimately became possible as the processes producing free oxygen (*e.g.*, hydrogen escape, carbon burial) exceeded the rate of oxygen consumption by different geological processes (*e.g.*, weathering, volcanic outgassing). Evidence from the ancient rock record suggests that atmospheric oxygenation occurred in steps, with a first rise of O_2 at 2.45–2.32 Ga and a second around 0.75–0.58 Ga (*e.g.*, Reinhard and Planavsky, 2022). The latter increase was a fundamental condition for the appearance of macroscopic animals. During the Phanerozoic, the oxygen concentration in the oceans also varied greatly, especially during great anoxic events of the Cenozoic (*e.g.*, Jenkyns, 2010). However, there remain significant unknowns regarding the timing and evolution of Earth surface oxygenation, especially for the first production of free oxygen by cyanobacteria sometime in the Archean and its initial accumulation in the atmosphere starting around 2.45 Ga.

Direct measurements of the chemical composition of the atmosphere in the past are impossible, and our understanding of the rise of oxygen in the atmosphere relies mainly on the sedimentary record and on redox proxies. The evidence for changes in redox state throughout geological times is multiple. The most decisive is probably the disappearance of mass independent fractionation of sulfur isotopes from the geological record (*e.g.*, Farquhar *et al.*, 2000). Moreover, several trace element proxies based on variations in metal concentrations and variations in their isotopic compositions have been developed to study the redox conditions in the ocean that can be directly correlated to the state of oxygenation in the atmosphere. For example, redox element enrichment, such as Mo, U and Cr, has been widely used to constrain the redox state of ancient oceans (*e.g.*, Brumsack, 2006). More recently, non-traditional stable isotopes have also been developed to help define the redox state of the ocean (*e.g.*, Eickmann *et al.*, 2018).

The redox behaviour of cerium and its unique ability to form Ce^{4+} ions among elements belonging to the rare Earth element (REE) have been used in the literature to study the redox conditions in modern and past environments (*e.g.*, Tostevin *et al.*, 2016). During magmatic processes, cerium is incompatible as other REE (affinity for the melt) and the main terrestrial reservoir for Ce is thus the continental crust. During oxidative weathering, Ce^{3+} is released into river waters and is later oxidised to Ce^{4+} (Elderfield *et al.*, 1990; German and Elderfield, 1990; Bau and Koschinsky, 2009). The chemical oxidation of cerium in seawater is believed to be mainly controlled by Mn and Fe cycling *via* Fe and Mn oxyhydroxides (Ohta and Kawabe, 2001; Bau *et al.*, 2014). Under oxidising conditions, Ce^{4+} is insoluble and readily absorbed onto particulates and Fe oxyhydroxides. Under reducing conditions, Ce^{3+} is soluble and behaves very similarly to its neighbours REE^{3+}, such as Pr and Nd. The redox dependent behaviour of cerium in seawater means that the residence time of Ce is short (less than 300 years) in oxic conditions.

1. Université Clermont Auvergne, CNRS, IRD, OPGC, Laboratoire Magmas et Volcans, 63000 Clermont-Ferrand, France
2. University Bretagne Occidentale-Brest, CNRS, IFREMER, Geo-Ocean, UMR 6538, IUEM, 29280 Plouzané, France
* Corresponding author (email: pierre.bonnand@univ-brest.fr)

Redox conditions in past oceans are classically investigated using Ce elemental anomalies. During the oxidation process, Mn-Fe oxyhydroxides are enriched in Ce relative to their neighbours and are characterised by positive Ce anomalies. Under oxidising conditions, cerium in seawater is thus depleted relative to its LREE neighbours (namely La, Pr and Nd), resulting in a negative Ce anomaly. On the other hand, under reducing conditions, Ce behaves similarly to other REE, resulting in no Ce anomaly. Although the Ce anomaly in natural environments has been largely used, the mechanisms responsible for the formation of elemental anomalies and the quantification of this process remain debated (*e.g.*, Bau *et al.*, 2014). For example, Ce anomalies can also be produced by bio-mediated reactions in anoxic environments (Kraemer and Bau, 2022).

Here we propose to use stable Ce isotopes to constrain the processes and the reaction rates responsible for the Ce behaviour in natural environments. Cerium has four stable isotopes of masses 136 (0.19 %), 138 (0.25 %), 140 (88.41 %) and 142 (11.15 %). The Ce isotopic composition is reported as the per mil variation from the Ce isotope standard LMV using the equation:

$$\delta^{142}Ce = \left(\frac{^{142}Ce/^{140}Ce_{sample}}{^{142}Ce/^{140}Ce_{LMV}} - 1\right) \times 1000 \qquad \text{Eq. 1}$$

We developed a triple spike method for measuring mass-dependent fractionation of Ce isotopes (Bonnand *et al.*, 2019). Cerium isotope variations in absorption experiments have also been performed (*e.g.*, Nakada *et al.*, 2013a). It has been shown that Ce isotopes are fractionated during Mn-Fe oxyhydroxide precipitation, with the precipitates enriched in light Ce isotopes. Natural samples have also been measured and ferromanganese nodules are a potential target to study redox changes in the palaeo-oceans (Nakada *et al.*, 2016). It has been proposed that aqueous speciation is the main factor controlling Ce isotope fractionation (Nakada *et al.*, 2017). To date, there is no investigation of the Ce isotopic fractionation during the Ce^{3+} to Ce^{4+} oxidation reaction. Accordingly, we performed two series of oxidation experiments to quantify the isotopic fractionation produced during the Ce^{3+} oxidation reaction, as well as measured the isotopic compositions of sediment samples characterised by different elemental cerium anomalies.

Results

The Ce concentration and isotopic composition of the oxidation experiments are presented in Table S-1. We performed two sets of experiments with varying oxidation duration (set 1, 3 minutes oxidation; set 2, 20 minutes). The Ce^{3+} was oxidised at room temperature, with varying amounts of a strong oxidising agent ($NaBrO_3$ + 10 M HNO_3). Varying the amount of oxidising agent enables partial oxidisation experiments with both Ce^{3+} and Ce^{4+} in solution (see Supplementary Information for details). The Ce^{3+} and Ce^{4+} fractions were chemically separated using ion-exchange chromatography (see Supplementary Information for details). In both sets of experiments, the amount of Ce^{3+} decreased from 3000 ng to 0 ng when oxidation proceeded, which translates to Ce/Ce* anomalies up to 0.1 as approximated by the Ce^{4+}/Ce_{TOT} ratio. The Ce^{3+} and Ce^{4+} fractions were analysed for their Ce isotopic composition. In the set 1 experiment (3 minutes), the Ce^{3+} fraction became isotopically heavy while oxidation proceeded. The Ce isotopic compositions varied from 0 ‰ to +0.4 ‰. The Ce^{4+} fraction was isotopically lighter than the Ce^{3+} fraction and became heavier while oxidation proceeded (Fig. 1a). In the 20 minutes experiments, the isotopic composition of the Ce^{3+} fraction was within error of the Ce^{4+} fraction (Fig. 1b) and very close to 0 ‰.

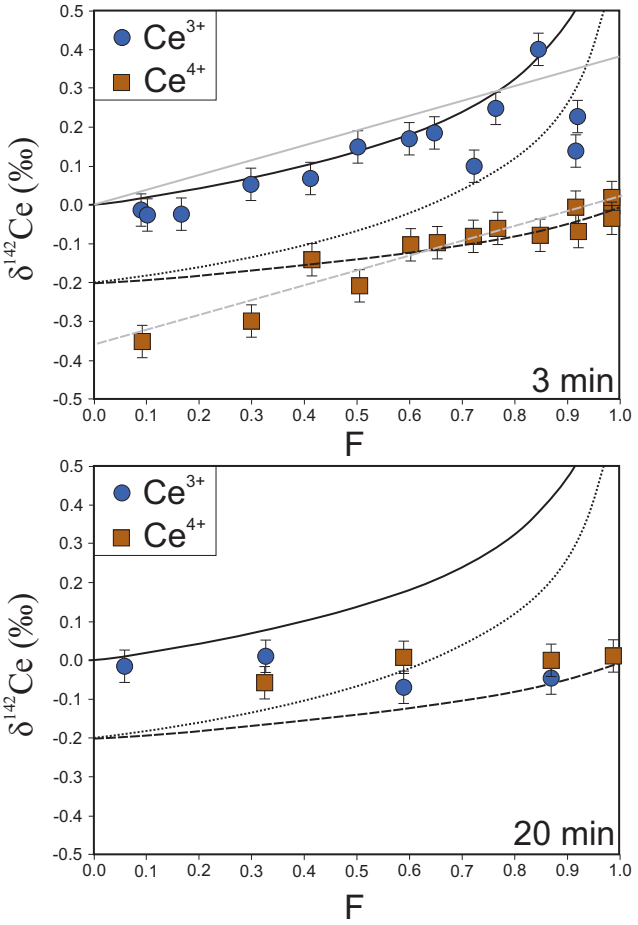

Figure 1 Ce isotopic composition for the Ce^{3+} and Ce^{4+} fractions in the oxidation experiments performed in this study. *F* is the fraction of Ce^{4+} produced during the reaction. The full, dotted and dashed lines are the Rayleigh fractionation models for the residual Ce^{3+}, the instantaneous Ce^{4+} and cumulated Ce^{4+}, respectively. The full and dashed grey lines are for the equilibrium model for the Ce^{3+} and Ce^{4+}, respectively. See text for details.

We have also analysed natural samples to determine whether samples with Ce elemental anomalies associated with redox reactions have a different isotopic composition compared to samples with Ce anomalies due to REE addition during alteration. The external reproducibility of our analytical technique has been determined by multiple measurements of two geological reference materials. To this end, BHVO-2 and GSP-2 were measured several times and we obtained $\delta^{142}Ce$ values of 0.087 ± 0.045 ‰ ($n = 4$) and 0.045 ± 0.044 ‰ ($n = 4$). Similarly, all geological samples (igneous and sedimentary rocks) analysed by Pourkhorsandi *et al.* (2021) have Ce isotopic compositions slightly heavier than their Ce standard. The Ce isotopic composition of natural samples analysed in this study are presented in Table S-2 and Figure 2. Analysed carbonate samples come from different locations (see Supplementary Information for details). They show the largest variations in $\delta^{142}Ce$ values (from 0.081 ‰ to 0.280 ‰). Banded iron formation (BIF) samples from the 3.22 Ga Moodies Group, Barberton Greenstone Belt, South Africa, have $\delta^{142}Ce$ values ranging from −0.055 ‰ to −0.007 ‰. Finally, two USGS Mn nodules (NOD-A1 and NOD-P1) are characterised by $\delta^{142}Ce$ values of 0.116 ‰ and 0.142 ‰, respectively. The carbonate samples show a covariation between Ce isotopic compositions and Ce elemental anomalies (Fig. 2).

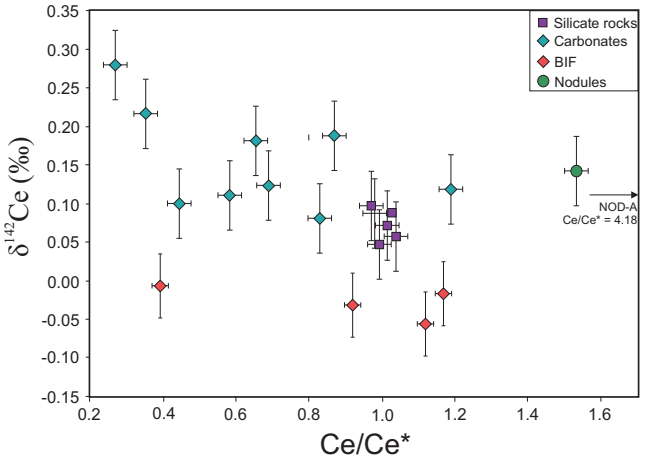

Figure 2 Ce isotopic compositions *versus* elemental cerium anomaly in the studied samples. The Ce anomaly is calculated using geometric extrapolation (see Barrat *et al.*, 2022) and the equation $Ce/Ce^* = Ce/(Pr^2/Nd)$ from Lawrence *et al.* (2006). See Table S-3 for details.

Discussion

We measured Ce isotope fractionations during oxidation of Ce^{3+} in two series of laboratory experiments, one lasting 3 minutes and one lasting 20 minutes. We observed that the amount of Ce^{4+} produced during the oxidation experiments was not dependent on the duration of the experiments but was strongly correlated to the amount of oxidising agent added to the original Ce^{3+}. As oxidation proceeded and the Ce^{3+} concentrations decreased, $\delta^{142}Ce$ values of the remaining unoxidised Ce^{3+} increased, indicating preferential oxidation of the lighter isotopes (Fig. 1). The isotopic composition of the Ce^{4+} produced during the reaction is isotopically light and varies from −0.32 ‰ to +0.08 ‰. The observed variations in $\delta^{142}Ce$, presented in Figure 1, could be explained by either a Rayleigh fractionation or an equilibrium fractionation model. As illustrated in Figure 1, the isotopic fractionation factor ($\alpha_{Ce3+-Ce4+}$) obtained for the experiments using a Rayleigh fractionation model is 1.0002. The fractionation factor obtained with an equilibrium fractionation model is 1.00035. Given the fact that the reaction is unidirectional, we prefer the Rayleigh fractionation model for explaining the observed variations. As shown in Figure 1, the Ce isotopic composition for the Ce^{4+} fractions at low degree of partial oxidation is not perfectly aligned with the Rayleigh fractionation model. This variability could be explained by two hypotheses: 1) the small amount of Ce^{3+} left in solution tends to re-equilibrate faster than at lower oxidation reaction rate; or 2) during the chemical separation of Ce^{3+} and Ce^{4+} fractions, there was isotopic fractionation occurring that could not be corrected using the triple spike technique. Nevertheless, the isotopic effect during oxidation reactions is clearly demonstrated in Figure 1. The isotopic variations observed after 20 minutes are different from those of the 3 minute experiments. Ce^{3+} and Ce^{4+} fractions have similar isotopic compositions after 20 minutes. This suggests that Ce^{3+} and Ce^{4+} had enough time to re-equilibrate in the solutions. It also implies that, at equilibrium, there is no isotopic difference between Ce^{3+} and Ce^{4+} in our medium. Importantly, the fractionation factors obtained for our experiments are similar to those of absorption experiments on Mn oxides (Nakada *et al.*, 2013b) which suggests that oxidation of Ce^{3+} is one of the main mechanisms responsible for Ce isotopic variations in natural aquifers. The obtained fractionation factors should be applicable to aquifers where abiotic Ce oxidation dominates.

Cerium isotopes are fractionated during oxidation reactions and it follows that, in natural environments, this process occurs. The Ce^{4+} is isotopically light and the Ce^{3+} remaining in solution is isotopically heavier. In natural waters, Ce^{4+} being insoluble is readily removed. It follows that the remaining Ce in solution will become progressively heavy during this process. It also suggests that precipitates of Ce^{4+} should be isotopically light compared to the initial isotopic composition. It should be noted that the 20 minute experiments show that, at equilibrium, there is no isotopic fractionation between Ce^{3+} and Ce^{4+} in solution. In order to preserve the oxidation reaction signature in natural environments, it is thus important that the Ce^{4+} fraction is readily removed from the system. Although seawater samples have not been measured yet, and isotopic variations observed in our experiments may not be directly applicable to natural environments, we speculate that, because of oxidation reactions and subsequent removal of isotopically light Ce^{4+}, seawater should be isotopically heavy compared to the continental crust. This, of course, is variable in time, and stable Ce isotope variations in ancient sediments could be a powerful tool to study oxidation of past oceans and the rise of oxygen in the atmosphere.

In order to quantify the variability of Ce isotopic compositions in natural systems, a number of natural samples have been measured (eight carbonates, four banded iron formations and two Mn nodules). The carbonate samples analysed span a large range of elemental Ce anomalies (0.24 to 1.08) and are characterised by variable Ce isotopic compositions. As illustrated in Figure 2, there is a covariation between elemental Ce anomaly and mass dependent Ce isotopic composition in the analysed carbonates. It is widely accepted that negative Ce anomalies in sediments are interpreted as reflecting oxic conditions. The negative co-variation between Ce/Ce* and $\delta^{142}Ce$ in carbonates indicates that the Ce anomaly is, indeed, associated with redox reactions. As Ce/Ce* decreases, the Ce isotopic composition becomes heavier, which is consistent with oxidation reactions driving the appearance of the negative Ce anomaly.

Four banded iron formations from the 3.22 Ga Moodies Group (Barbeton Greenstone Belt, South Africa) have been analysed for their Ce isotopic composition. The BIF samples were also characterised by large negative elemental Ce anomalies. Amongst BIF samples, however, no Ce isotopic variations are observed. This suggests that the production of negative Ce anomaly is not linked to redox reactions. The Ce anomalies in the Moodies BIF analysed in this study have previously been linked to a late fluid circulation event not related to the conditions during deposition of these chemical sediments (Bonnand *et al.*, 2020). The results obtained in this study agree with this finding. In details, the Ce isotopic compositions in the BIF samples analysed in this study are slightly negative compared to the continental crust value. This result could be interpreted to reflect the incorporation of isotopically light Ce^{4+} into the BIF lattice. Although this hypothesis should be confirmed with further studies, it clearly highlights the complementarity between elemental Ce anomaly and the Ce isotopic composition to track the presence of atmospheric oxygen in marine chemical archives such as BIFs or carbonates.

Finally, the two analysed Mn nodules are characterised by large elemental positive Ce anomalies (1.39 and 3.78; Table S-2). Their Ce isotopic compositions are amongst the heaviest samples analysed in this study. Although the source of Ce in Mn nodules can be heterogenous (*e.g.*, seawater, hydrothermal and pore fluids), it suggests that these samples do record redox reactions within the Ce cycle in the Ocean and this result agrees with previously published results on ferromanganese deposits (Nakada *et al.*, 2016). Fe-Mn oxyhydroxides actively oxidise Ce by surface precipitation which suggests that the Ce incorporated in the Mn nodules can come from isotopically fractionated

seawater. It is likely that the ambient seawater was isotopically heavier than the Ce isotopic composition recorded in these samples (Nakada *et al.*, 2013b). It is also important to note that the analysed nodules are mixed-type nodules and Ce isotopes may also record secondary processes, such as diagenetic reactions.

Conclusions

The results presented here demonstrate that Ce isotopes are a powerful redox proxy for past and present environments. The co-variations between Ce anomaly and stable Ce isotopic composition indicate that Ce isotopes can be used to demonstrate the nature of Ce elemental anomalies. It will allow the distinction between redox driven Ce anomaly and elemental anomalies driven by secondary processes not related to redox conditions. It could also be useful to distinguish between Ce anomalies produced with and without the presence of oxygen. Mass dependent Ce isotope variations can also be coupled to radiogenic Ce. Using the La-Ce systematics, the La fractionation from Ce in old sediments can be dated which means that Ce anomaly and mass dependent Ce isotope variations are some of the few redox proxies that can be directly dated, providing exceptional insights into the early Earth oxygenation history.

Acknowledgements

We would like to thank Inga Kohler for the Banded iron formation samples. Delphine Auclair is also thanked for looking after the TIMS laboratory at Laboratoire Magmas et Volcans in Clermont-Ferrand. We would like to thank Dennis Kraemer and two anonymous reviewers for their constructive criticisms that helped us to improve this manuscript. We would like to thank Stefan Lalonde for numerous discussions about Ce isotopes. This project has received funding from the European Research Council (ERC) under the European Union's Horizon 2020 research and innovation program (grant agreement no. 6822778 to M.B.). This is Laboratory of Excellence ClerVolc contribution n°629.

Editor: Claudine Stirling

Additional Information

Supplementary Information accompanies this letter at https://www.geochemicalperspectivesletters.org/article2340.

Cite this letter as: Bonnand, P., Boyet, M., Bosq, C. (2023) Stable cerium isotopes as a tracer of oxidation reactions. *Geochem. Persp. Let.* 28, 27–30. https://doi.org/10.7185/geochemlet.2340

References

Barrat, J.-A., Bayon, G., Lalonde, S. (2022) Calculation of cerium and lanthanum anomalies in geological and environmental samples. *Chemical Geology* 615, 121202. https://doi.org/10.1016/j.chemgeo.2022.121202

Bau, M., Koschinsky, A. (2009) Oxidative scavenging of cerium on hydrous Fe oxide: Evidence from the distribution of rare earth elements and yttrium between Fe oxides and Mn oxides in hydrogenetic ferromanganese crusts. *Geochemical Journal* 43, 37–47. https://doi.org/10.2343/geochemj.1.0005

Bau, M., Schmidt, K., Koschinsky, A., Hein, J., Kuhn, T., Usui, A. (2014) Discriminating between different genetic types of marine ferro-manganese crusts and nodules based on rare earth elements and yttrium. *Chemical Geology* 381, 1–9. https://doi.org/10.1016/j.chemgeo.2014.05.004

Bonnand, P., Israel, C., Boyet, M., Doucelance, R., Auclair, D. (2019) Radiogenic and stable Ce isotope measurements by thermal ionisation mass spectrometry. *Journal of Analytical Atomic Spectrometry* 34, 504–516. https://doi.org/10.1039/C8JA00362A

Bonnand, P., Lalonde, S.V., Boyet, M., Heubeck, C., Homann, M., Nonnotte, P., Foster, I., Konhauser, K.O., Köhler, I. (2020) Post-depositional REE mobility in a Paleoarchean banded iron formation revealed by La-Ce geochronology: A cautionary tale for signals of ancient oxygenation. *Earth and Planetary Science Letters* 547, 116452. https://doi.org/10.1016/j.epsl.2020.116452

Brumsack, H.-J. (2006) The trace metal content of recent organic carbon-rich sediments: Implications for Cretaceous black shale formation. *Palaeogeography, Palaeoclimatology, Palaeoecology* 232, 344–361. https://doi.org/10.1016/j.palaeo.2005.05.011

Eickmann, B., Hofmann, A., Wille, M., Bui, T.H., Wing, B.A., Schoenberg, R. (2018) Isotopic evidence for oxygenated Mesoarchaean shallow oceans. *Nature Geoscience* 11, 133–138. https://doi.org/10.1038/s41561-017-0036-x

Elderfield, H., Upstill-Goddard, R., Sholkovitz, E.R. (1990) The rare earth elements in rivers, estuaries, and coastal seas and their significance to the composition of ocean waters. *Geochimica et Cosmochimica Acta* 54, 971–991. https://doi.org/10.1016/0016-7037(90)90432-K

Farquhar, J., Bao, H., Thiemens, M. (2000) Atmospheric Influence of Earth's Earliest Sulfur Cycle. *Science* 289, 756–758. https://doi.org/10.1126/science.289.5480.756

German, C.R., Elderfield, H. (1990) Application of the Ce anomaly as a paleoredox indicator: The ground rules. *Paleoceanography* 5, 823–833. https://doi.org/10.1029/PA005i005p00823

Jenkyns, H.C. (2010) Geochemistry of oceanic anoxic events. *Geochemistry, Geophysics, Geosystems* 11, Q03004. https://doi.org/10.1029/2009GC002788

Kraemer, D., Bau, M. (2022) Siderophores and the formation of cerium anomalies in anoxic environments. *Geochemical Perspectives Letters* 22, 50–55. https://doi.org/10.7185/geochemlet.2227

Lawrence, M.G., Jupiter, S.D., Kamber, B.S. (2006) Aquatic geochemistry of the rare earth elements and yttrium in the Pioneer River catchment, Australia. *Marine and Freshwater Research* 57, 725–736. https://doi.org/10.1071/MF05229

Nakada, R., Takahashi, Y., Tanimizu, M. (2013a) Isotopic and speciation study on cerium during its solid-water distribution with implication for Ce stable isotope as a paleo-redox proxy. *Geochimica et Cosmochimica Acta* 103, 49–62. https://doi.org/10.1016/j.gca.2012.10.045

Nakada, R., Tanimizu, M., Takahashi, Y. (2013b) Difference in the stable isotopic fractionations of Ce, Nd, and Sm during adsorption on iron and manganese oxides and its interpretation based on their local structures. *Geochimica et Cosmochimica Acta* 121, 105–119. https://doi.org/10.1016/j.gca.2013.07.014

Nakada, R., Takahashi, Y., Tanimizu, M. (2016) Cerium stable isotope ratios in ferromanganese deposits and their potential as a paleo-redox proxy. *Geochimica et Cosmochimica Acta* 181, 89–100. https://doi.org/10.1016/j.gca.2016.02.025

Nakada, R., Tanaka, M., Tanimizu, M., Takahashi, Y. (2017) Aqueous speciation is likely to control the stable isotopic fractionation of cerium at varying pH. *Geochimica et Cosmochimica Acta* 218, 273–290. https://doi.org/10.1016/j.gca.2017.09.019

Ohta, A., Kawabe, I. (2001) REE(III) adsorption onto Mn dioxide (δ-MnO_2) and Fe oxyhydroxide: Ce(III) oxidation by δ-MnO_2. *Geochimica et Cosmochimica Acta* 65, 695–703. https://doi.org/10.1016/S0016-7037(00)00578-0

Pourkhorsandi, H., Debaille, V., de Jong, J., Armytage, R.M.G. (2021) Cerium stable isotope analysis of synthetic and terrestrial rock reference materials by MC-ICPMS. *Talanta* 224, 121877. https://doi.org/10.1016/j.talanta.2020.121877

Reinhard, C.T., Planavsky, N.J. (2022) The History of Ocean Oxygenation. *Annual Review of Marine Science* 14, 331–353. https://doi.org/10.1146/annurev-marine-031721-104005

Tostevin, R., Shields, G.A., Tarbuck, G.M., He, T., Clarkson, M.O., Wood, R.A. (2016) Effective use of cerium anomalies as a redox proxy in carbonate-dominated marine settings. *Chemical Geology* 438, 146–162. https://doi.org/10.1016/j.chemgeo.2016.06.027

Geochemical Perspectives Letters

Stable cerium isotopes as a tracer of oxidation reactions

P. Bonnand, M. Boyet, C. Bosq

Supplementary Information

The Supplementary Information includes:

- Materials and Methods
- Tables S-1 to S-3
- Supplementary Information References

Materials and Methods

The silicate samples are international rock standards (BCR-2, W2, GSP-2, BHVO-2 and AGV-2). Their REE concentrations are reported in Table S-1.

Several carbonate samples analysed in this study are international rock standards (JDo-1, Cal-S, BCS CRM 513 and BCS CRM 393). I27 is a Neoproterozoic carbonate sample from Islay (Scotland). B08 is a modern ooids sample from the Bahamas. C171 is an oolitic limestone from the Caswell Bay oolite. Their chemical compositions have been previously investigated (Bonnand *et al.*, 2013). Pt1 and Pt5 are two upper Jurassic carbonates studied by Olivier and Boyet (2006). The REE concentrations and the Ce anomalies (Ce/Ce*) are presented in Tables S-1 and S-2, respectively. The samples are a combination of limestones and dolomite and have been selected to cover a large range of elemental Ce anomalies. The Ce/Ce* values are calculated using geometric extrapolation and the equation $Ce/Ce^* = Ce/(Pr^2/Nd)$ from Lawrence *et al.* (2006).

The BIF samples have been previously investigated for their chemical composition and their radiogenic cerium isotopic composition (Bonnand *et al.*, 2020). The samples are from the 3.22 Ga Moodies Group of the Barberton Greenstone Belt which is comprised of sand- and siltstone, subordinate conglomerate and volcanics, and minor ferruginous sediment that were mostly deposited in shallow-marine and/or terrestrial settings (*e.g.*, Heubeck, 2019). The samples have been selected to cover the large Ce anomaly previously described at this locality.

The Mn nodule samples are two USGS standards (NOD-A1 and NOD-P1). They are believed to be from mixed sources (a combination of hydrogenetic and diagenetic formation). The Ce anomaly measured for the Mn nodules samples are presented in supplementary Table S-1.

Chemical dissolution procedure for natural samples

The dissolution procedures vary depending on the nature of the samples. For silicate samples, the dissolution was achieved by adding a HF–HNO_3 mixture (3:1 ratio) to the sample powders. The beakers were placed on the hotplate at 90 °C for at least 24 h. The samples were then treated with 6 M HCl to remove the fluorides formed during the dissolution. For the carbonate samples, a weak room temperature acetic acid (0.5 M) dissolution procedure was used in order to avoid the dissolution of detrital components. The BIF and nodule samples were dissolved using a 6 M HCl room temperature dissolution procedure.

Triple spike

In order to correct for mass fractionation during chemical separation and measurements on the mass spectrometer, a triple spike method was developed and is fully described in Bonnand *et al.* (2019). The Ce isotopic composition is reported as the per mil variation from the Ce isotope standard LMV using the equation:

$$\delta^{142}\mathrm{Ce} = \left(\frac{^{142}\mathrm{Ce}/^{140}\mathrm{Ce}_{\mathrm{sample}}}{^{142}\mathrm{Ce}/^{140}\mathrm{Ce}_{\mathrm{LMV}}} - 1 \right) \times 1000. \qquad \text{Eq. S-1}$$

The LMV Ce standard has been prepared from AMES metal (Bonnand *et al.*, 2019) and is available on request.

Chemical separation procedures

The chemical separation method used in this study is modified after Tazoe *et al.* (2007), Li *et al.* (2015), Bellot *et al*. (2015) and Bonnand *et al.* (2019). The chemical separation developed to separate the Ce fraction from silicate matrices involved three column chemistries. For the first step of the separation procedure, the samples were loaded onto 1 mL of AG50 X8 200–400 mesh resin in 2.5 N HCl. The REE stuck to the resin while the main cations were eluted from the resin. The first step of the procedure was designed to isolate the REEs from the main cations of the matrix. The first chemistry also allowed the separation between REE and Ba (one of the main isobaric interference). During this first chemical separation, Ba was then eluted in 2 M HNO_3 and the REE were eluted in 6 M HCl. The second column procedure was designed to separate Ce^{4+} from the other REE (La and Nd) and followed the procedure proposed by Tazoe *et al.* (2007). The chemical separation procedure was tested for blanks

and yield. We obtained yields that were 99.9 % for this chemistry and the blanks were less than 0.2 ng of Ce. The oxidation of Ce^{3+} to Ce^{4+} was achieved with 0.5 mL of $NaBrO_3$ (20 mM) in 10 M HNO_3. The samples were loaded in 10 M HNO_3 + $NaBrO_3$ onto 0.2 mL LnSpec Eichrom resin (50–100 µm). During this step of the chemical procedure, Ce^{4+} stuck to the resin while all REE^{3+} were eluted in the loading solution. The Ce fraction (present as Ce^{4+}) was eluted in 6 M HCl + H_2O_2. Finally, the samples were then processed through the first step of the chemistry (AG50 X8, 200–400 mesh) to make sure the Ce fraction was free of any remaining matrix cations. For the seawater derived samples (carbonates, banded iron formations and Mn nodules), another column was performed prior to the protocol described above. For the carbonate samples, the samples were processed through a TRU spec resin in 1 M HNO_3. In this chemistry, Ce sticks to the resin and the Ca from the matrix does not. For the banded iron formation and the Mn nodules, Fe was removed by processing the samples through an anionic column. To this end, the samples were loaded onto AG1 X8 resin in 6 M HCl. In these conditions, Fe sticks to the resin and the cerium fraction does not. The total procedural blank was better than 0.4 ng of Ce.

Oxidation experiments

The oxidation experiments were performed at room temperature in the clean laboratory. The oxidation experiments are based on the chemical separation procedure performed in the step 2 of the protocol described above, but rather than using excess perbromic acid to ensure complete oxidation of Ce^{3+} to Ce^{4+}, variable concentrations of perbromic acid were employed. The two redox couples involved in this oxidation reaction are Ce^{3+}/Ce^{4+} and BrO_4^-/BrO_3^-. The oxidative capacity of perbromic acid has been described in Appelman (1969). The oxidation reaction can be summarised as:

$$2Ce^{3+} + BrO_4^- + 2H^+ \rightarrow 2Ce^{4+} + BrO_3^- + H_2O. \qquad \text{Eq. S-2}$$

For the partial oxidation experiments, a Ce^{3+} solution was first dried down in a beaker. In order to achieve variable degrees of oxidation, we added different amount of $NaBrO_3$ in 10 M HNO_3 to the samples (from 0.0008 to 0.04 mmol $NaBrO_3$). Two series of experiments were performed with two durations of oxidation (3 and 20 minutes). The 3 minutes experiments were performed in three different sessions in the laboratory. The two fractions (Ce^{3+} and Ce^{4+}) were then isolated by processing the solution through the step 2 of the chemical purification procedure without further treatment. The partially oxidised solutions were directly loaded onto the ln resin without additional processing. During this chemical procedure, the solutions (with both Ce^{3+} and Ce^{4+}) were loaded in 10 M HNO_3 + variable $NaBrO_3$ onto 0.2 mL LnSpec Eichrom resin (50–100 µm). During this step of the chemical procedure, the fraction of Ce^{3+} is directly collected because it is eluted in the loading solution. The Ce^{4+} fraction sticks to the resin and is then collected later, once a solution of 6 M HCl + H_2O_2 is added. After separation, the Ce^{4+} fraction was aliquoted and the Ce concentration was measured on the quadrupole ICP-MS

(Agilent 7500). The possibility of Ce loss *via* precipitation of CeO_2(s) is excluded considering the recently determined solubility constant for nanoparticulate CeO_2(s) (Plakhova *et al.*, 2016) that supports strong undersaturation in our experimental procedures. The amount of Ce^{3+} was thus calculated assuming a 100 % recovery (see above subsection 'Chemical separation procedure'). The Ce^{3+} and Ce^{4+} fractions were then spiked with the requisite amount of Triple spike. In order to remove the Na added during the oxidation procedure, the samples were cleaned using a single chromatography procedure using cation resin AG50 X8 (described above as the first step of the chemical procedure for natural samples) and measured on the TIMS Triton Plus, following the procedures described below.

Mass spectrometry

Isotopic measurements were performed on a ThermoScientific Thermal Ionisation Mass spectrometer Triton Plus (TIMS) at the Laboratoire Magmas et Volcans. The Ce standards and samples were analysed in oxide forms using the double filament technique. The Ce fraction was loaded in HCl onto outgassed Re wire together with 0.5 µL of 1 M H_3PO_4. The cup configuration used is described in Bonnand *et al.* (2019) and allows the simultaneous measurements of Ce isotopes (^{136}Ce, ^{138}Ce, ^{140}Ce and ^{142}Ce) and half masses necessary for the tailing correction. The Ce masses and the tailing are measured with 10^{11} and 10^{13} Ω resistors, respectively. Typical runs on the mass spectrometer consist of 27 blocks of 20 cycles with 8.462 seconds integration time. Each block started with a baseline measurement of 30 seconds. The gain calibrations for the 10^{11} and 10^{13} Ω resistors were performed daily using the ThermoScientific software built in gain routine (at 0.33 V). The Ce isotopic composition of the samples and standards was determined offline but baseline and gain corrections were performed online with the ThermoScientific software. The deconvolution procedure for both unspiked and spiked runs can be divided in three main steps: tail correction on mass ^{136}Ce and ^{138}Ce, oxide corrections and mass bias fractionation corrections and is performed offline.

The reproducibility of our mass spectrometry technique has been assessed by multiple measurements of our Ce_{LMV} standard without chemical separation ($\delta^{142}Ce_{LMV}$ = 0.000 ± 0.037 ‰ (2 s.d.; n = 5). The accuracy was assessed with analyses of the Ce_{LMV} standard after chemical purification for each sample's matrices. The data is given in Table S-3. The results obtained with the three separation procedures (silicate, carbonate and Fe-rich) are all within error of the unpurified Ce_{LMV} standard solution (see Table S-3). The external reproducibility of our analytical technique has been determined by multiple measurements of two geological reference material. To this end, BHVO-2 and GSP-2 were measured several times and we obtained δ^{142}Ce values of 0.087 ± 0.045 ‰ (n = 4) and 0.045 ± 0.044 ‰ (n = 4), respectively. The value obtained for the JDo-1 Dolomite standard is slightly heavier than the published values by Nakada *et al.* (2019). It is however important to note that the normalising standard is different and direct comparison of δ^{142}Ce value is impossible.

Supplementary Tables

Table S-1 Ce quantities and Ce isotopic compositions in the oxidation experiments (See text for details of the experimental settings). The 2 s.e. is the internal error of the Ce measurements.

Sample name	Oxidation time (min)	Ce^{3+} (ng)	Ce^{4+} (ng)	Ce^{4+}/Ce_{TOT}	$\delta^{142}Ce(III)$ (‰)	2 s.e.	$\delta^{142}Ce(IV)$ (‰)	2 s.e.
OE5	3	bdl	3000	1.00	n.d.	n.d.	-0.010	0.004
OE6	3	247	2753	0.92	0.141	0.007	0.006	0.005
OE7	3	700	2300	0.77	0.245	0.006	-0.061	0.009
OE8	3	2100	900	0.30	0.053	0.010	-0.295	0.007
OE9	3	2721	279	0.09	-0.015	0.011	-0.347	0.006
OE10	3	0	3000	1.00	n.d.	n.d.	0.028	0.004
OE11	3	4	2996	1.00	n.d.	n.d.	0.022	0.007
OE12	3	39	2961	0.99	n.d.	n.d.	0.017	0.006
OE13	3	232	2768	0.92	0.223	0.004	-0.061	0.007
OE14	3	832	2168	0.72	0.101	0.004	-0.081	0.008
OE15	3	1046	1954	0.65	0.182	0.007	-0.109	0.014
OE16	3	1485	1515	0.51	0.147	0.010	-0.207	0.009
OE17	3	451	2549	0.85	0.399	0.005	-0.074	0.011
OE18	3	1196	1804	0.60	0.169	0.006	-0.108	0.007
OE19	3	1760	1240	0.41	0.073	0.019	-0.139	0.005
OE20	3	2497	503	0.17	-0.024	0.004	n.d.	n.d.
OE21	3	2696	304	0.10	-0.022	0.004	n.d.	n.d.
OE22	20	bdl	2988	1.00	n.d.	n.d.	0.017	0.006
OE23	20	386	2613	0.87	-0.021	0.004	0.026	0.007
OE24	20	1228	1771	0.59	-0.055	0.006	0.030	0.010
OE25	20	2021	978	0.33	0.042	0.007	-0.059	0.008
OE26	20	2821	178	0.06	0.016	0.007	n.d.	n.d.

bdl, below detection limit; n.d., not determined.

Table S-2 Ce isotopic compositions and elemental Cerium anomaly (Ce/Ce*) in the studied samples. The 2 s.e. is the internal error of the Ce measurements.

Sample name	δ^{142}Ce (‰)	2 s.e.	Ce/Ce*
AGV2	0.069	0.005	1.01
BCR-2	0.058	0.005	1.04
BHVO-2	0.087	0.004	1.02
W2	0.096	0.007	0.97
GSP2	0.045	0.004	0.99
Jdo-1	0.337	0.005	0.27
Cal-S	0.100	0.012	0.44
BCS CRM 393	0.179	0.005	0.65
BCS CRM 513	0.123	0.005	0.69
C171	0.217	0.007	0.35
Pt1	0.111	0.006	0.58
Pt5	0.081	0.013	0.83
B08	0.186	0.015	0.87
I27	0.119	0.009	1.19
average carbonates	0.161	0.160†	
IK14-3	-0.032	0.004	0.92
IK14-12b	-0.055	0.005	1.12
IK14-18	-0.007	0.005	0.39
14-37	-0.015	0.004	1.17
average BIF	-0.027	0.042†	
NOD-A1	0.116	0.005	4.18
NOD-P1	0.142	0.004	1.53
average nodules	0.129	0.037†	

†2 s.d.

Table S-3 REE concentrations for the analysed samples and Ce isotopic composition for analytical tests.

Table S-3 (.xlsx) is available for download from the online version of this article at https://doi.org/10.7185/geochemlet.2340.

Supplementary Information References

Appelman, E.H. (1969) Perbromic acid and perbromates: synthesis and some properties. *Inorganic Chemistry* 8, 223–227. https://doi.org/10.1021/ic50072a008

Bellot, N., Boyet, M., Doucelance, R., Pin, C., Chauvel, C., Auclair, D. (2015) Ce isotope systematics of island arc lavas from the Lesser Antilles. *Geochimica et Cosmochimica Acta* 168, 261–279. https://doi.org/10.1016/j.gca.2015.07.002

Bonnand, P., James, R.H., Parkinson, I.J., Connelly, D.P., Fairchild, I.J. (2013) The chromium isotopic composition of seawater and marine carbonates. *Earth and Planetary Science Letters* 382, 10–20. https://doi.org/10.1016/j.epsl.2013.09.001

Bonnand, P., Israel, C., Boyet, M., Doucelance, R., Auclair, D. (2019) Radiogenic and stable Ce isotope measurements by thermal ionisation mass spectrometry. *Journal of Analytical Atomic Spectrometry* 34, 504–516. https://doi.org/10.1039/C8JA00362A

Bonnand, P., Lalonde, S.V., Boyet, M., Heubeck, C., Homann, M., Nonnotte, P., Foster, I., Konhauser, K.O., Köhler, I. (2020) Post-depositional REE mobility in a Paleoarchean banded iron formation revealed by La-Ce geochronology: A cautionary tale for signals of ancient oxygenation. *Earth and Planetary Science Letters* 547, 116452. https://doi.org/10.1016/j.epsl.2020.116452

Heubeck, C. (2019) The Moodies Group—a High-Resolution Archive of Archaean Surface Processes and Basin-Forming Mechanisms. In: Kröner, A., Hofmann, A. (Eds.) *The Archaean Geology of the Kaapvaal Craton, Southern Africa*. Regional Geology Reviews. Springer, Cham., 133–169. https://doi.org/10.1007/978-3-319-78652-0_6

Lawrence, M.G., Jupiter, S.D., Kamber, B.S. (2006) Aquatic geochemistry of the rare earth elements and yttrium in the Pioneer River catchment, Australia. *Marine and Freshwater Research* 57, 725–736. https://doi.org/10.1071/MF05229

Li, C.-F., Wang, X.-C., Li, Y.-L., Chu, Z.-Y., Guo, J.-H., Li, X.-H. (2015) Ce-Nd separation by solid-phase micro-extraction and its application to high-precision $^{142}Nd/^{144}Nd$ measurements using TIMS in geological materials. *Journal of Analytical Atomic Spectrometry* 30, 895–902. https://doi.org/10.1039/C4JA00328D

Nakada, R., Asakura, N., Nagaishi, K. (2019) Examination of analytical conditions of cerium (Ce) isotope and stable isotope ratio of Ce in geochemical standards. *Geochemical Journal* 53, 293–304. https://doi.org/10.2343/geochemj.2.0567

Olivier, N., Boyet, M. (2006) Rare earth and trace elements of microbialites in Upper Jurassic coral- and sponge-microbialite reefs. *Chemical Geology* 230, 105–123. https://doi.org/10.1016/j.chemgeo.2005.12.002

Plakhova, T.V., Romanchuk, A.Y., Yakunin, S.N., Dumas, T., Demir, S., Wang, S., Minasian, S.G., Shuh, D.K., Tyliszczak, T., Shiryaev, A.A., Egorov, A.V., Ianov, V.K., Kalmykov, S.N. (2016) Solubility of Nanocrystalline Cerium Dioxide: Experimental Data and Thermodynamic Modeling. *The Journal of Physical Chemistry C* 120, 22615–22626. https://doi.org/10.1021/acs.jpcc.6b05650

Pourmand, A., Dauphas N., Ireland T.J. (2012) A novel extraction chromatography and MC-ICP-MS technique for rapid analysis of REE, Sc and Y: Revising CI-chondrite and Post-Archean Australian Shale (PAAS) abundances. *Chemical Geology* 291, 38–54. https://doi.org/10.1016/j.chemgeo.2011.08.011

Tazoe, H., Obata, H., Gamo, T. (2007) Determination of cerium isotope ratios in geochemical samples using oxidative extraction technique with chelating resin. *Journal of Analytical Atomic Spectrometry* 22, 616–622. https://doi.org/10.1039/b617285g